ORIGINAL PAPER

Flood risk mapping and crop-water loss modeling using water footprint analysis in agricultural watershed, northern Iran

Maziar Mohammadi[1] · Hamid Darabi[2] · Fahimeh Mirchooli[1] · Alireza Bakhshaee[3] · Ali Torabi Haghighi[2]

Abstract

Spatial information on flood risk and flood-related crop losses is important in flood mitigation and risk management in agricultural watersheds. In this study, loss of water bound in agricultural products following damage by flooding was calculated using water footprint and agricultural statistics, using the Talar watershed, northern Iran, as a case. The main conditioning factors on flood risk (flow accumulation, slope, land use, rainfall intensity, geology, and elevation) were rated and combined in GIS, and a flood risk map classified into five risk classes (very low to very high) was created. Using average crop yield per hectare, the amount of rice and wheat products under flood risk was calculated for the watershed. Finally, the spatial relationships between agricultural land uses (rice and wheat) and flood risk areas were evaluated using geographically weighted regression (GWR) in terms of local R^2 at sub-watershed scale. The results showed that elevation was the most critical factor for flood risk. GWR results indicated that local R^2 between rice farms and flood risk decreased gradually from north to south in the watershed, while no pattern was detected for wheat farms. Potential production of rice and wheat in very high flood risk zones was estimated to be 7972 and 18,860 tons, on an area of 822 ha and 7218 ha, respectively. Loss of these crops to flooding meant that approximately 34.04 and 12.10 million m^3 water used for production of wheat and rice, respectively, were lost. These findings can help managers, policymakers, and watershed stakeholders achieve better crop management and flood damage reduction.

Keywords Flood damages · Water footprint · Crop water loss · Flood risk management · GIS · Talar watershed

✉ Ali Torabi Haghighi
  Ali.TorabiHaghighi@oulu.fi

Extended author information available on the last page of the article

1 Introduction

Flooding is one of the most devastating and costly natural hazards. It has severe socio-economic and environmental consequences, including destroying farmland, reducing crop yield, and causing regional freshwater shortages (Mind'je et al. 2019). Flooding can only occur not only in lowland areas but also in mountainous environments. Analysis of flooding and its relationships with explanatory variables can help water managers identify the most effective variable in flooding (Hosseini et al. 2020). Therefore, identification of flood-prone areas and of the most influential conditioning factors is an essential tool in mitigating the effects of flooding (Khosravi et al. 2016). Various models have been developed to estimate potential flood risk areas and simulate flow (Darabi et al. 2019; Rahmati et al. 2019). However, some of these models cannot simulate and evaluate flood risk under different scenarios, while in some heterogeneity of input data, e.g., on land use and geology, makes determining the threshold flow more difficult (Zhao et al. 2018). Other models have limitations especially in ungauged and extensive areas. As a solution, multi-criteria analysis (MCA) is a useful first step in mapping and evaluating flood risk areas. In MCA, it is possible to select, evaluate, and combine relevant factors to map the final flood risk (Santos et al. 2019). Understanding the particular interrelationships between water and food can enhance the resilience of water-food systems, since food security is highly associated with water and both are affected by a changing climate. Therefore, quantifying the effects of floods on crop production, and consequently on food security, are important (Pacetti et al. 2017). These detrimental effects can influence food availability, identified by the Food and Agriculture Organization of the United Nations (FAO) as a pillar of food security (FAO 2015). Therefore, it is important to manage irrigated and rainfed agricultural systems in light of the relationship between agricultural land uses and flood-prone areas, in order to maintain the ecosystem service of food production. In an MCA approach to identify the effect of flooding on irrigated and rainfed agricultural crops in the present study, the "water footprint" (WF) concept introduced by Hoekstra (2003) was used. The WF of an agricultural crop is defined as the total volume of water (rainfall or irrigation) used to produce the product (Hoekstra 2009). The damage caused by floods to crop production can thus be converted to WF as a complementary indicator. Some previous case studies have evaluated the effects of flood events on food availability, e.g., Pacetti et al. (2017) calculated the damage of flooding to agricultural areas in Bangladesh and Pakistan in terms of lost calories. However, previous studies have estimated flood damage using conventional statistical analyses, which produce average parameter estimates, and thus spatial variations in flood damage to crops and their associated WF have been ignored. A more sophisticated analytical technique was needed to overcome this limitation. In response, geographical weighted regression (GWR), a statistical model, was developed to investigate spatial correlation and heterogeneity (Xia et al. 2018). GWR examines spatially non-stationary parameters, so model performance is improved by reducing spatial autocorrelations. In recent years, GWR has been widely employed to good effect in different fields, to analyze, e.g., groundwater quantity (Taghipour Javi et al. 2014; Almeida et al. 2018), rainfall and environmental indices (Georganos et al. 2017; Ahmadi et al. 2018b; Salimi et al. 2018), land surface temperature (Kalota 2017; Zhao et al. 2018), urban and regional differences (Dadashpoor et al. 2019; Duncan et al. 2019) and ecology and human geography (Tu 2011; Li et al. 2018).

The staple foods in Iran are rice-based and wheat-based foods (Nejad et al. 2011; Karizaki 2016) and the Talar watershed in Mazandaran province, northern Iran, is one of the most important regions for domestic cultivation of these crops. Therefore, these two major

crops and the Talar watershed were selected as a case for calculating the risk of potential crop-water losses due to flooding using the WF approach. Floods cause severe damage to agricultural land and residential areas in Mazandaran province (Darabi et al. 2020), with 70% of available credit going to repair the damage caused by flooding (Sadeghi-Pouya et al. 2017). In this MCA study, the crop damage and associated water loss caused by flooding were calculated by integrating satellite images, field data, and agricultural for northern Iran. Specific objectives of the study were to: (i) create a flood risk map using conditioning factors; (ii) determine the water losses associated with flood-related losses of wheat and rice, through the WF approach; and (iii) explore the spatial relationships between area of flood risk classes and areas of main crops (e.g., wheat and rice) in the study watershed using the GWR technique.

2 Materials and methods

2.1 Study area

The Talar watershed in northern Iran (36° 36′–36° 46′ N; 55° 23′–54° 31′ E) extends along the coast of the Caspian Sea, to which the Talar river drains in a south-north direction (Fig. 1). This mountainous watershed (mean altitude ~ 1800 masl) covers 2055 km² and has a Mediterranean rainfall regime, with mean annual precipitation of 552.7 mm, the majority falling in spring. Rice and wheat, which together account for about 23% of agricultural land, are the main crops (Maghsood et al. 2019). The terrain is mountainous, with steep slopes covering more than 60% of the area. The main land uses are rangeland, forest,
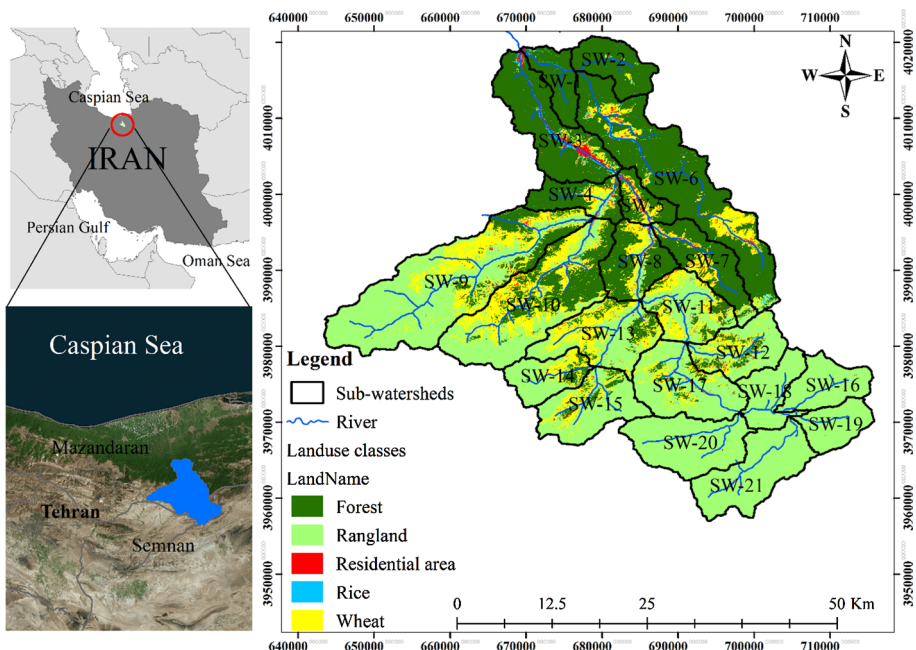

Fig. 1 Maps showing the location of the Talar watershed in northern Iran

rainfed agriculture, irrigated agriculture, and residential area (Shooshtari and Gholamalifard 2015). The watersheds in northern Iran have experienced drastic changes due to mining activities, road construction, and residential development. Large areas of forest and rangelands have been converted to cropland, orchards, and residential areas in the past four decades (Kavian et al. 2018; Pirnia et al. 2019). These changes have affected the hydrological response, ultimately altering runoff volume and flow regime in watersheds (Haghighi et al. 2020). In the Talar watershed, recent decades due to intensive deforestation and land use change, the potential of runoff generation and peak flow have been increased 12.38% and 41.8%, respectively (Khaleghi 2017). In Table 1, characteristics of rainfall station are presented.

2.2 Data sets

For the purposes of this study, Talar watershed border and sub-watersheds of the Talar River were delineated using digital elevation model (DEM) with resolution 30 m and Arc-SWAT extension 2012.10_4.21v. A land use map of the Talar watershed was extracted using Landsat 8/Operational Land Imager (OLI) image (21.06.2016) and supervised classification algorithm in the ENVI 5.3 (Torabi Haghighi et al. 2018). Five land use types were identified: forest, rangeland, irrigated agriculture, rainfed agriculture, and residential area.

The spatial variability in flood risk was determined based on six factors (Fig. 2): slope (S), elevation (E), flow accumulation (F), geology (G), land use (L), and rainfall intensity (R), see Eq. (1), which have direct important impacts on flood risk (Kourgialas and Karatzas 2011, 2016; Kazakis et al. 2015). These factors were prepared as six thematic maps, which were then combined into one final flood risk map using linear algebraic function and their weights in the GIS environment. Factors F and G are qualitative, whereas factors S, E, and R are considered quantitative. The factors were classified into five flood risk zones (FRZ): very low, low, moderate, high, and very high. Jenk's natural breaks method was applied to classify quantitative (numerical) factors, whereas qualitative factors were classified based on their effect in flood recharging. For example for factor L (land use), forest was classified as very low flood risk, but residential area as very high flood risk. For each classified factor's flood risk rating, a numerical value was allocated (very low (1), low (2), moderate (5), high (8), and very high (10)) (Kourgialas and Karatzas 2016).

Since all factors do not have the same effect on flooding condition, two types of effects were considered: minor effect, where a change in one factor has an indirect effect on another factor (allocated 0.5 points), and major effect, where a change in one factor has a direct effect

Table 1 Rainfall station characteristics

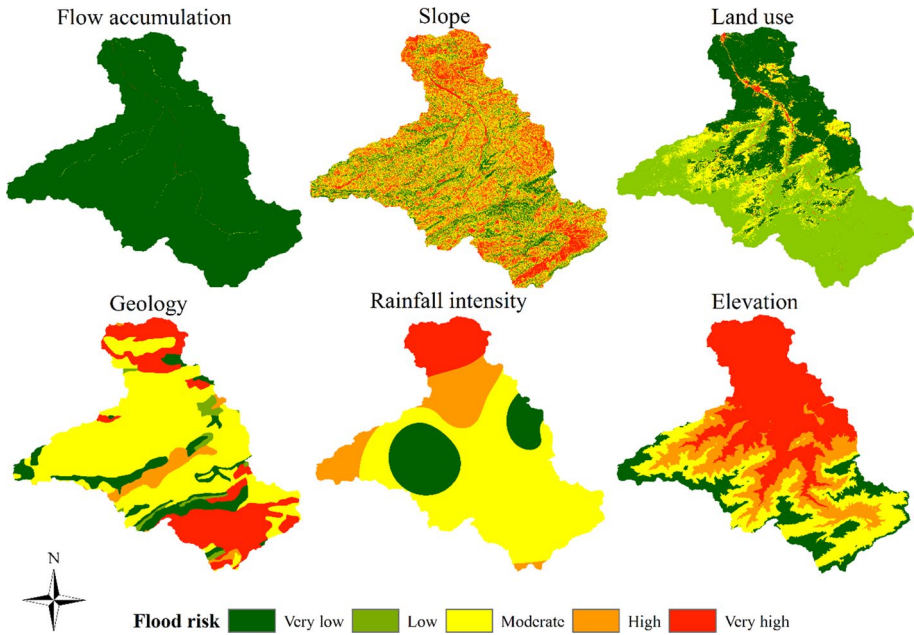| Station name	X	Y	Elevation	Fornie	Erosivity
Alasht	678,538	3,996,861	396	29.45	382.24
Darzikola	698,086	3,995,431	546	22.59	234.24
Golafshan	673,335	4,031,900	2268	94.64	3792.61
Paland	671,409	3,987,865	464	21.27	209.54
Sangdeh	701,131	3,993,651	764	26.57	316.05
Shirgha	669,274	4,019,097	1077	34.23	504.72
Soleymantangeh	700,663	4,013,990	593	21.58	215.35

Fig. 2 Maps indicating the intensity of different conditioning factors for flood risk in the Talar watershed

on another factor (allocated 1 point). The final rating of each factor was calculated by adding together the points allocated to minor and major effects (Table 2). All factors, FRZs, and points scores used were based on previous studies (Kourgialas and Karatzas 2011; Kazakis et al. 2015). Evaluation of the literature indicated that the six selected factors provide necessary and useful information for improving flood risk modeling (Zerger 2002).

The final score for each factor (Table 2) was obtained by multiplying proposed weight of effect (RL) by factor rate (FR). Finally, a flood risk map of the Talar watershed was prepared using linear summation method of factors (FREGLS) in GIS as (Kourgialas and Karatzas 2011):

$$\text{FREGLS} = \sum x_i w_i = F w_F + S w_S + L w_L + R w_R + G w_G + E w_E \qquad (1)$$

Table 2 Minor and major effects of flood risk conditioning factors and their interactions on flood recharge

Factor	Minor effect	Major effect	Score
Rainfall intensity (R)	(L)	(F)	1.5 points (1 minor + 1 major)
Slope (S)		(L), (F)	2.0 points (0 minor + 2 major)
Flow accumulation (F)	(S)	(L)	1.5 points (1 minor + 1 major)
Elevation (E)	(S)	(G), (F), (R), (L)	4.5 points (1 minor + 4 major)
Land use (L)	(S), (G)	(R), (F)	3.0 points (2 minor + 2 major)
Geology (G)		(F), (L), (S)	3.0 points (0 minor + 3 major)

where x_i is the thematic map of each factor i, w_i is the weight of each factor i and *F, S, L, R, G, E* are flow accumulation factor, slope factor, land use factor, rainfall intensity factor, geology factor, and elevation factor, respectively.

Using DEM with spatial resolution 30 m, the elevation (*E*) was classified, and a slope (S) map was produced using the 3D Analyst tool in GIS. Land use and land cover affect the volume of runoff, with a direct impact on both the time for which soil receives rainfall and the amount (Kazakis et al. 2015).

The geology (*G*) and land formation-based classification of the study area were produced based on the Iranian geological map (Geological Survey of Iran, 1997). Permeable geological formations with high porosity and fractures reduce runoff coefficient and runoff volume, whereas fine-grained and impermeable formations increase runoff volume and flood risk (Table 2).

Flow (*F*) accumulation was generated using DEM and the spatial analyst tool in the GIS environment. In this map, pixels with higher values have more hydrological connections with other pixels, and thus make a higher contribution on flood risk.

In order to calculate rainfall intensity factor (*R*), precipitation data from seven rainfall stations in the Talar watershed were used. The map of rainfall intensity was created using Modified Fournier Index (MFI) (Morgan 2005), calculated as:

$$\text{MFI} = \sum_{i=1}^{12} \frac{p_i^2}{P} \tag{2}$$

where *p* is the mean monthly rainfall for month *i* ($1 \leq I \leq 12$) and *P* is the mean annual rainfall. MFI shows the average monthly rainfall for stations, calculated using interpolated spline method. This method is a useful way to indicate spatial variation in, e.g., rainfall, especially in data-limited situations (Lloyd 2005). MFI can be used for the Mediterranean rainfall regime, in which flashy floods and overflow of stream banks are common (Belmonte and Beltrán 2001; Kourgialas and Karatzas 2016). All thematic maps were prepared with spatial resolution of 30 m × 30 m and summed with the Raster calculator tool in the GIS environment considering Eq. 1.

2.3 Flood damage to agricultural products and associated water loss

The effect of flood damage on agricultural products in terms of crop and water (irrigation water) loss was estimated using spatial data such as land use maps and agricultural statistics (Brémond and Grelot 2013; Giang et al. 2020). Determining the damage to agriculture due to flooding involved estimating loss of agricultural products, taking into account the topography, land use, and characteristics of cultivated crops in the study area (Pacetti et al. 2017). The effect of flooding on crop production includes loss of the crop itself, reduced food security, loss of energy, and loss of water used for production of the crop. Thus, the percentage of different land uses in each sub-watershed in the Talar watershed was calculated. According to the annual agricultural organization report (Ahmadi et al. 2018a), irrigated agriculture in this region is mostly rice, grown near the main river, while rainfed agricultural lands is mainly devoted to wheat production. Thus, rice and wheat land were assumed for irrigated and rainfed agriculture in the study area, respectively. In order to estimate agricultural production, total amount of rice and wheat crops was calculated based on potential for agricultural production per unit area in sub-watersheds (Ahmadi et al. 2018a, b). For estimating agricultural product loss, all rice and wheat farms located in high and

very high flood risk areas were considered potential agriculture crop losses (Kourgialas and Karatzas 2016).

The amount of water loss associated with crop losses was estimated using WF (Eq. 3). This indicator represents direct or indirect use of water to produce goods or services and includes three types of WF: blue (using surface or groundwater), green (using rainwater), and grey (the amount of water to assimilate pollutants) (Hoekstra 2017). Flood damage to agricultural land represents loss of water, especially blue water used for, e.g., irrigation, which directly impacts future agricultural production. Therefore, in the present study, the amount of water footprint loss (WFL) was calculated based on water requirement of the crop (irrigation or rainfall) as:

$$PAP = A \times P \tag{3}$$

$$WFL = WF_i \times A_i \tag{4}$$

where PAP is the potential of agriculture production, A *is* the area (ha) under rice and wheat production, P is the potential production of each crop (ton/ha), A_i is the wheat or rice area (ha) on land in high and very high flood risk classes, and WF_i is the water footprint of wheat or rice ($m^3\ kg^{-1}$), as suggested by Mekonnen and Hoekstra, (2011).

2.4 Geographically weighted regression

Geographically weighted regression (GWR) was used to assess relationships between agricultural land uses (rice and wheat) and flood risk areas at sub-watershed scale. This model can explore the spatial relationship between dependent and independent variables considering no-stationarity properties of targeted phenomena (Stewart Fotheringham et al. 1996). The GWR equation is (Fotheringham et al. 1998):

$$y_j = \beta_0(u_j, v_j) + \sum_{i=1}^{p} \beta_j(u_j, v_j) x_{ij} + \varepsilon_j \tag{5}$$

where (u_j, v_j) is the coordinates for location j, $\beta i\ (u_j, v_j)$ is the local regression coefficient for independent variables χ_i at location j, $\beta_0(u_j, v_j)$ is the intercept, ε_j is an error term, and y_j is the value of the dependent variable for the j th sample. Local R^2 in the GWR model is an indicator of how dependent and independent variables are fitted together. The higher the value of local R^2, the lower the residual square sum, indicating a higher correlation (Wu et al. 2017).

3 Results and discussion

Table 3 shows the conditioning factors and sub-classification of flood risk zones and their proposed rating. The effects of the different conditioning factors were as follows:

Flow accumulation A key factor in flood risk, as high value of this layer represents concentrated flow, and consequently higher flood risk.

Slope An important spatial factor for identification of flood risk through surface runoff velocity and vertical percolation (Rahmati et al. 2016). The highest slope is assigned the highest rating (Table 3). In this study, the slope was extracted in percent based on the digital elevation model. The slope factor influence on the water velocity and plays a major

Table 3 Influential conditioning factors in flood risk classification in the Talar watershed and their weights

Factors	Domain of effect	Flood risk zone	Proposed weight of effect (RL)	Rate (FR)	Weighted rating (FR*RL)	Total weight	Percentage (%)
Flow accumulation	0–120,471	Very low	1	1.5	1.5	39	9.68
	120,471–421,201	Low	2	1.5	3		
	421,201–801,392	Moderate	5	1.5	7.5		
	801,392–1,346,148	High	8	1.5	12		
	1,346,148–2,614,982	Very high	10	1.5	15		
Slope (%)	0–12.02	Very low	1	2	2	52	12.90
	12.02–19.97	Low	2	2	4		
	19.97–28	Moderate	5	2	10		
	28–37.57	High	8	2	16		
	37.57–73.21	Very high	10	2	20		
Land use	Forest	Very low	1	3	3	78	19.35
	Rangeland	Low	2	3	6		
	Rainfed agriculture	Moderate	5	3	15		
	Irrigated agriculture	High	8	3	24		
	Residential area	Very high	10	3	30		
Rainfall intensity (MFI)	21.27–25.61	Very low	1	1.5	1.5	39	9.68
	25.61–28.47	Low	2	1.5	3		
	28.47–32.91	Moderate	5	1.5	7.5		
	32.91–38.83	High	8	1.5	12		
	38.83–48.36	Very high	10	1.5	15		
Geology	Sandstone, Limestone	Very low	1	3	3	78	19.35
	Conglomerate, Shale and marl, Piedmont fan and valley terrace, Gypsiferous marl, Swamp and marsh, Shale, tuff, Sandstone, Sandy limestone,	Low	2	3	6		
		Moderate	5	3	15		
		High	8	3	24		
	Basaltic volcanic	Very high	10	3	30		

Table 3 (continued)

Factors	Domain of effect	Flood risk zone	Proposed weight of effect (RL)	Rate (FR)	Weighted rating (FR*RL)	Total weight	Percentage (%)
Elevation (m)	213–1036	Very low	1	4.5	4.5	117	29.03
	1036–1619	Low	2	4.5	9		
	1619–2141	Moderate	5	4.5	22.5		
	2141–2646	High	8	4.5	36		
	2646–4003	Very high	10	4.5	45		
Sum						403	100.00

role in flooding in highlands and reflect a constant threat in lowlands due to gentle slopes. The slope map was created in ArcGIS 10.5 to quantify topographic controls on flood conditions.

Land use Influences flooding and inundation level through altering infiltration, changing the relationship between groundwater and surface water, and debris flow (Kazakis et al. 2015; Areu-Rangel et al. 2019). Runoff and consequently flood conditions vary considerably under different LULC patterns. In the Talar watershed area, the main land uses were found to be rangeland and forest (Fig. 1).

Rainfall intensity Expressed using MFI, it ranged from 21.27 to 48.36, with higher values in the north of the watershed and lower values in central and southern areas (Fig. 2).

Geology Can amplify and extenuate the frequency and magnitude of floods (Kazakis et al. 2015). Some formations, such as Karst, significantly affect flood generation, so a lower rating is associated with higher infiltration capacity and fewer flood events.

Elevation Plays a vital role in controlling surface flow movement and flood depth (Rahmati et al. 2019). In the Talar watershed, elevation varies between 213 to 4003 m asl, with the highest values in the south and the lowest in the north. Elevation was identified as the most important factor in flood risk in the study area (Table 3), as in other study areas (Tehrani et al. 2015; Ozkan and Tarhan 2016; Wang et al. 2017). The weighting for elevation was higher than for rainfall intensity and inferred intensification of rainfall with increasing elevation, confirming findings in previous studies (Kourgialas and Karatzas 2011).

In order to identify areas at risk of flooding in the Talar watershed, conditioning maps (Fig. 2) were combined in a single map (Fig. 3). This revealed areas with very high flood risk (VHFR) and high flood risk (HFR) in northern sub-watersheds. Overall, flood risk appeared to be more intense in the north, and around the river network in the south of the watershed. This part of the watershed mostly consists of forest, agriculture, and residential areas. Green areas and forests are reported to reduce flood risk, because of their infiltration
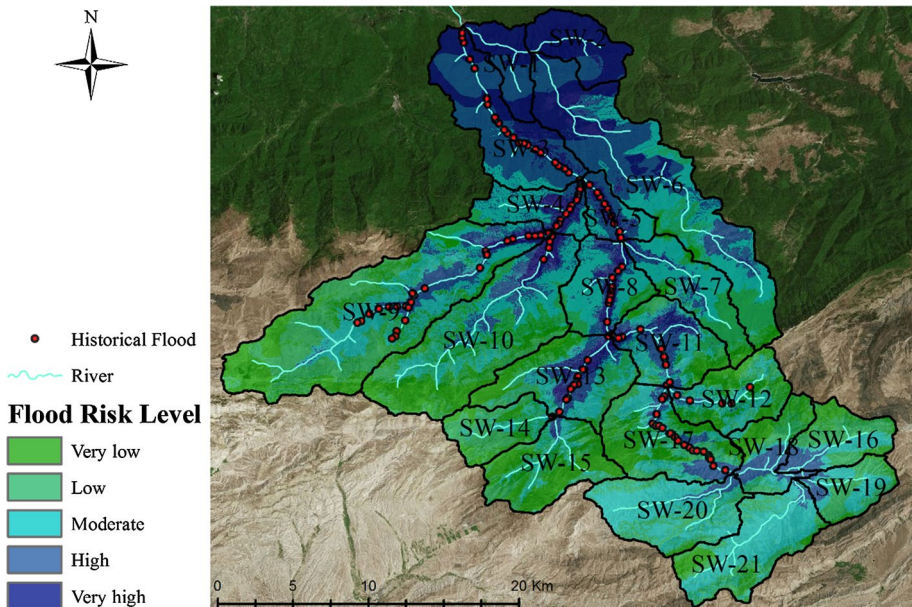

Fig. 3 Flood risk map for the Talar watershed at sub-watershed scale

capacity and evapotranspiration potential (Gaston et al. 2005; Smith et al. 2011; Warhurst et al. 2014). However, the actual effect can differ, as the results of this study showed. First, the design of vegetation cover might be inappropriate from the flood mitigation viewpoint, so that green lands are convex and higher than adjacent roads, increasing the flood risk, as reported for Shanghai, China (Wang et al. 2017). Second, the elevation factor, which was identified as the most influential conditioning factor in the Talar watershed, is low in forested and northern parts of the watershed. Some eastern, western, and southern parts of the watershed, which were found to have low and very low flood risk (LFR–VLFR) (Fig. 3), are mostly covered by rangeland and have high elevation.

3.1 Validation

In order to verify the final flood risk map, 134 historical flood points were used (Fig. 3). The positions of observed flooding points were determined through document obtained from regional water company of Mazandaran and field observation, interviews with local people, and water tail evaluation, and recorded by global positioning system (GPS) conducted in 2017. The overall accuracy of the flood risk map was assessed for two classes, HFR and VHFR. The location of historical floodplains in different flood level risk classes was determined by overlaying historical flood risk points on the flood risk map and using the spatial analyst tool (to extract values to points). A total of 111 out of 134 flooded points was found to be located in the high and very high flood risk classes in the final flood risk map, which means that the overall accuracy of the flood risk map was 83%.

3.2 Flood risk and damage

The area of agricultural land in flood risk zones was calculated for each sub-watershed. In order to compute the potential water loss, the area and yield of the rice and wheat crops had to be determined. Based on the land use map, an area of 2516.44 ha of the Talar watershed was occupied by rice and 31,260.71 ha by wheat (corresponding to 17% of watershed area). As the basin-based information on yield was not available in the study area, so we considered the average of province for our study. The average yield of wheat (1.73 ton ha^{-1}) and rice (4.79 ton ha^{-1}) in Mazandaran province (Ahmadi et al. 2018a) was assumed.

The area of rice and wheat farmland in high and very high flood risk areas (HFR-VHFR) in each sub-watershed is mapped in Fig. 4, and corresponding data are summarized in Table 4. For rice farmland, the highest flood risk level was observed for sub-watersheds 1 and 2, with area 369.79 ha and 310.69 ha, respectively. For wheat, the highest flood risk level was observed for sub-watersheds near the outlet. In general, a large proportion of land under rice (613.67 ha) and wheat (12,750.45 ha) was found to be exposed to VHFR flood risk damage and inundation in the 500 m buffer zone of the Talar river.

Assuming the flooded agricultural areas lost all cultivated crops and that all agricultural areas were productive, the potential losses of rice and wheat, derived by the intersection of land use and flood risk areas were calculated to be 7972.05 tons and 18,860.65 ton, respectively. The associated irrigation water loss through rice and wheat crops, calculated as WF, was 12.10 and 34.04 million m^3 (MCM), respectively, or over 46 MCM in total (Table 5 and Fig. 5).
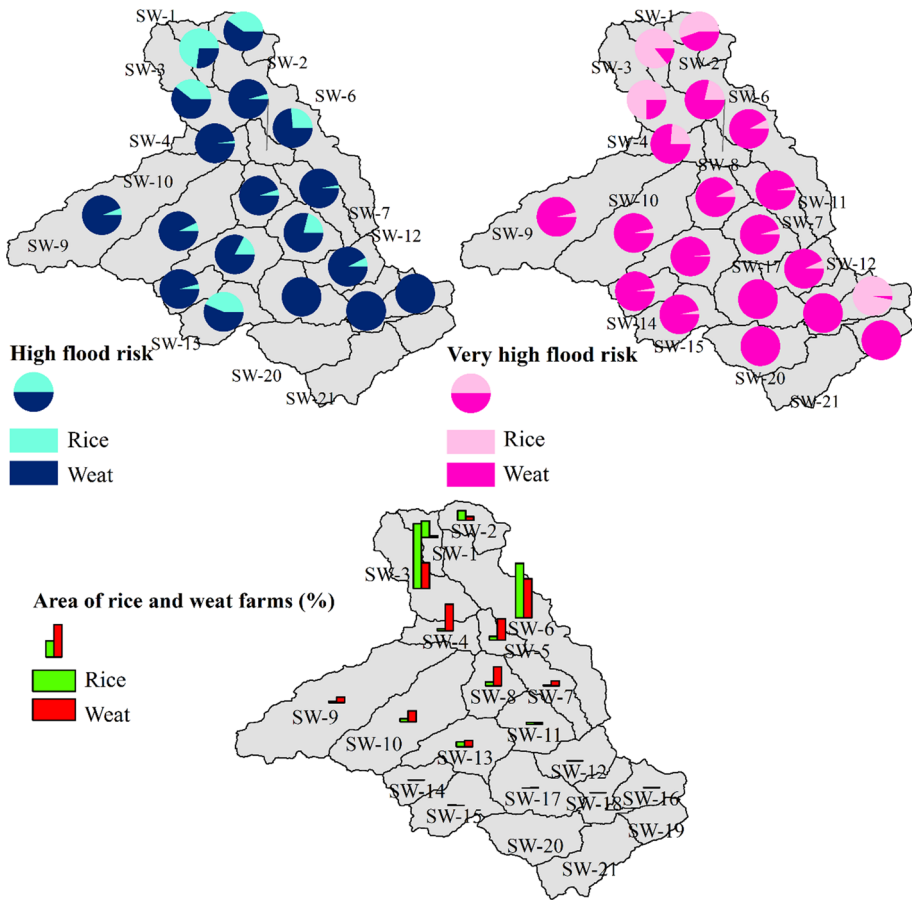
Fig. 4 Area of rice and wheat zones over the high and very high flood risk at sub-watershed scale

3.3 Spatial relationship between areas of flood risk zones and crops

Spatial statistics can play a key role in environmental studies. Our GWR model results indicated that the value of local R^2 varied from 0.11 to 0.82 in the study area (Fig. 6). In the case of rice-HFR, the classes with high values of local R^2 were shown to be located in northern and central areas of the watershed, where the agricultural land use and residential areas are mostly located. For rice-VHFR, classes with medium and low values were shown to be located in the south of the watershed. In addition, the spatial distribution of local R^2 revealed a gradual decrease from north to south. In the case of wheat-HFR, the classes with high values of local R^2 were located in eastern and south-western parts of the watershed, while other parts of the watershed had low value of local R^2 (Fig. 6). Classes with high and medium values were located in the south of the watershed. These findings indicate that the flood potential map is sensitive to location, which is consistent with other studies (Sim et al. 2014; Wang et al. 2017; Purwaningsih et al. 2018). Flood risk zoning in agricultural watershed with intensive rainfall and floods has received attention from agricultural policy-makers and planners because understanding of flooding conditions enhance their responses

Table 4 Area (ha) of rice and wheat crops in the Talar watershed found to be under high and very high flood risk level

Sub-watershed	Flood risk				Area croplands		
	High		Very high				
	Rice	Wheat	Rice	Wheat	Rice	Wheat	Rice and wheat
SW-1	92.98	34.80	4.93	0.82	97.91	35.62	133.52
SW-2	54.26	80.57	4.01	3.25	58.28	83.82	142.09
SW-3	369.79	568.37	307.19	102.65	676.98	671.03	1348.01
SW-4	11.97	586.62	65.09	209.77	77.06	796.39	873.45
SW-5	21.05	472.63	78.82	290.51	99.87	763.15	863.01
SW-6	310.69	863.38	150.91	1816.75	461.59	2680.13	3141.72
SW-7	3.12	105.34	16.28	487.73	19.40	593.08	612.47
SW-8	22.57	420.27	57.33	742.56	79.90	1162.83	1242.74
SW-9	7.63	124.65	36.79	965.49	44.42	1090.14	1134.57
SW-10	18.53	241.11	63.07	1601.03	81.60	1842.13	1923.74
SW-11	9.68	36.15	14.90	309.19	24.59	345.34	369.93
SW-12	0.09	1.06	4.52	60.68	4.61	61.75	66.35
SW-13	29.04	138.27	9.01	544.86	38.05	683.12	721.17
SW-14	0.03	0.63	0.78	27.38	0.81	28.00	28.81
SW-15	1.26	1.62	0.78	22.95	2.04	24.57	26.61
SW-16	0.00	0.00	8.41	0.27	8.41	0.27	8.68
SW-17	0.00	7.64	0.00	31.04	0.00	38.67	38.67
SW-18	0.00	0.08	0.00	1.56	0.00	1.64	1.64
SW-19	0.00	0.00	0.00	0.34	0.00	0.34	0.34
SW-20	0.00	0.00	0.00	0.09	0.00	0.09	0.09
SW-21	0.00	0.00	0.00	0.00	0.00	0.00	0.00
Total	952.68	3683.20	822.83	7218.91	1775.51	10,902.11	12,677.62

to flood risk. In current study, the efficiency of the water footprint analysis for spatial flood risk mapping and crop-water loss modeling was investigated and the resulting map was interpreted with the rice and wheat farms agricultural productions. Results demonstrated that the employed model had excellent performance in agricultural watershed.

4 Conclusions

Due to the special topographic and climatic conditions of Mazandaran province, agricultural lands are always in danger of annual flood damages. Rice farms are located near the river to provide cost-effective water supply, so these lands are faced with flood risk in comparison to other areas. As a result, assessment of spatial flood risk to cropland is important for better flood risk management and damage reduction in agricultural watersheds. In the present study, a flood risk map was prepared for the Talar watershed based on MCA method, one of the most important irrigated and rain-fed agricultural areas in Iran, where flooding occurs periodically. The map was created using six conditioning factors (flow accumulation, slope, land use, rainfall intensity, geology, and elevation). Of these,

Table 5 Potential production of rice and wheat and water footprint (WF) loss at sub-watershed scale in the Talar watershed

Sub-watersheds	Potential production (ton)		WF loss (MCM)		
	Rice	Wheat	Rice	Wheat	Total WF loss
SW-1	439.60	61.62	0.67	0.11	0.78
SW-2	261.66	145.00	0.40	0.26	0.66
SW-3	3039.64	1160.87	4.62	2.10	6.71
SW-4	346.00	1377.76	0.53	2.49	3.01
SW-5	448.40	1320.24	0.68	2.38	3.06
SW-6	2072.56	4636.62	3.15	8.37	11.52
SW-7	87.09	1026.02	0.13	1.85	1.98
SW-8	358.76	2011.70	0.54	3.63	4.18
SW-9	199.47	1885.94	0.30	3.40	3.71
SW-10	366.41	3186.89	0.56	5.75	6.31
SW-11	110.40	597.44	0.17	1.08	1.25
SW-12	20.68	106.82	0.03	0.19	0.22
SW-13	170.83	1181.80	0.26	2.13	2.39
SW-14	3.63	48.45	0.01	0.09	0.09
SW-15	9.18	42.50	0.01	0.08	0.09
SW-16	37.76	0.47	0.06	0.00	0.06
SW-17	0.00	66.90	0.00	0.12	0.12
SW-18	0.00	2.85	0.00	0.01	0.01
SW-19	0.00	0.58	0.00	0.00	0.00
SW-20	0.00	0.16	0.00	0.00	0.00
SW-21	0.00	0.00	0.00	0.00	0.00
Total	7972.05	18,860.65	12.11	34.04	46.15
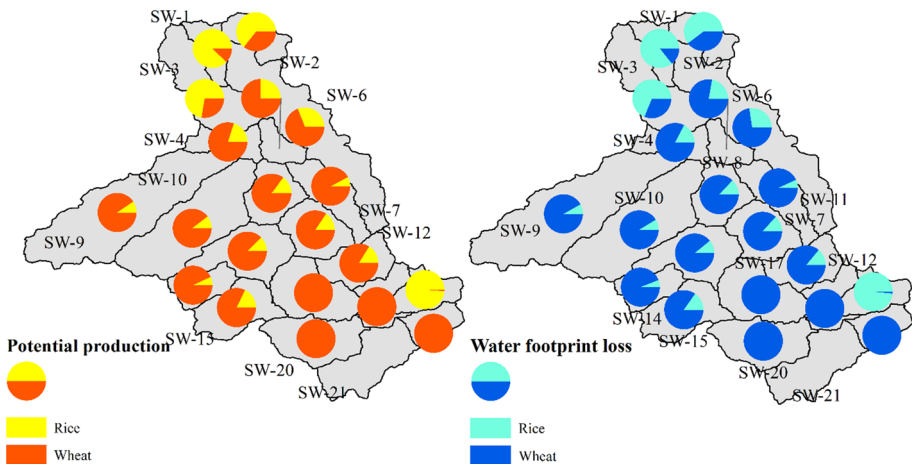
Fig. 5 Potential production and water footprint loss at sub-watershed scale
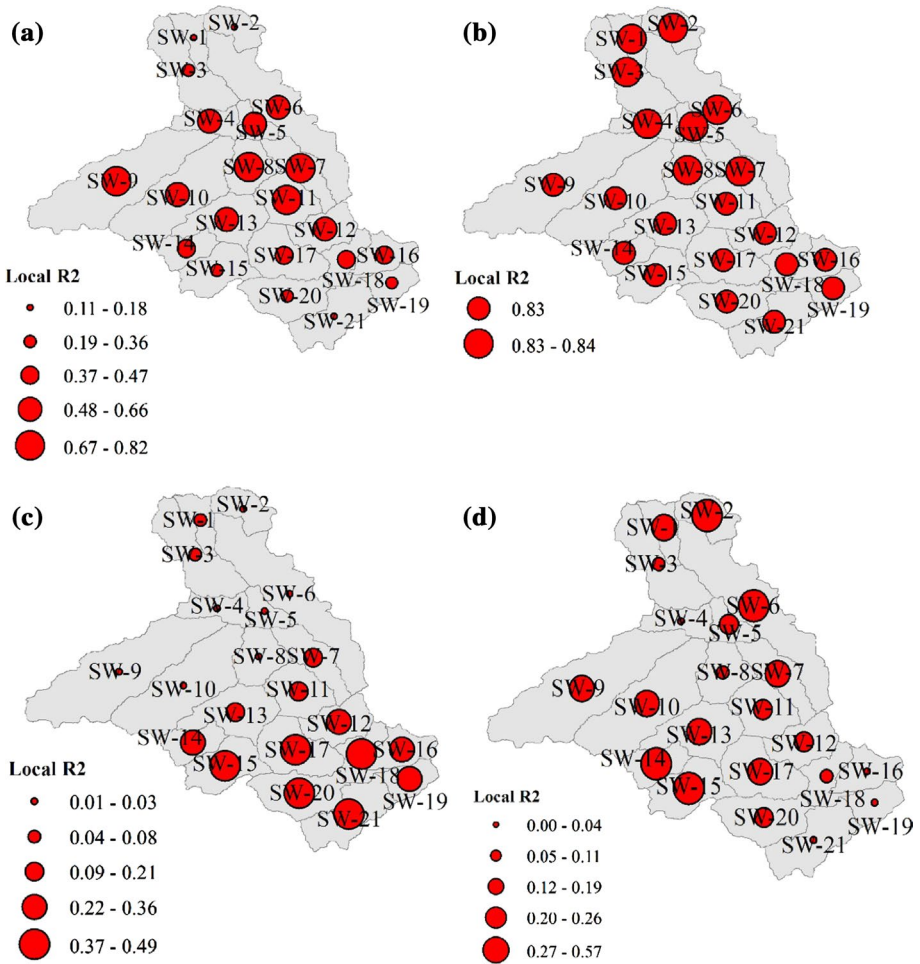
Fig. 6 Spatial correlation coefficient between high flood risk (HFR) and very high flood risk (VHFR) zones with production of rice (RP) and wheat (WP) at sub-watershed level, **a** RP-HFR, **b** RP-VHFR, **c** WP-HFR, and **d** WP-VHFR

elevation best explained frequent flood occurrence. Verification of the flood risk map using historical data on flood events revealed 83% accuracy for the map. The results showed that 31% of the total area of Talar watershed is under very high and high flood risk, and that 38% of its cropland (rice, wheat) is under high-very high flood risk. The irrigation water loss associated with crop losses to flooding was estimated to be 46.15 MCM, based on WF analysis. In this paper, in order to prepare flood risk map and to estimate agricultural water-crop losses, we integrated MCA modeling with water footprint method and agricultural statistics. Since the flood as a natural-human destructive phenomenon depends on various environmental factors, the use of multi-criteria analysis modeling reduces this complexity. Also, using the water footprint method, water loss can be calculated for agricultural crop losses caused by flood damage. In addition to agricultural products, water is also wasted, and this is an important issue in water resources management that has received less attention in flood damage studies. Also, in order to better understand the relation between flood

risk area and agricultural lands at sub-watershed scale, using geographically weighted regression (GWR) was used. These results are valuable information for flood damage reduction and sustainable agriculture management planning in the Talar watershed and in similar cultivated watersheds under flood risk.

References

Ahmadi K, Ebadzadeh HR, Abdshahi H et al (2018) Annual agricultural statistics. Ministry of Agriculture-Jahad, Tehran

Ahmadi M, Kashki A, Dadashi A (2018) Spatial modeling of seasonal precipitation—elevation in Iran based on aphrodite database. Model Earth Syst Environ 4:619–633. https://doi.org/10.1007/s40808-018-0444-y

Areu-Rangel OS, Cea L, Bonasia R, Espinosa-Echavarria VJ (2019) Impact of urban growth and changes in land use on river flood hazard in Villahermosa, Tabasco (Mexico). Water 11:304

Belmonte AMC, Beltrán FS (2001) Flood events in Mediterranean ephemeral streams (ramblas) in Valencia region, Spain. CATENA 45:229–249

Brémond P, Grelot F (2013) Review article: economic evaluation of flood damage to agriculture—review and analysis of existing methods. Nat Hazards Earth Syst Sci 13:2493–2512. https://doi.org/10.5194/nhess-13-2493-2013

Dadashpoor H, Azizi P, Moghadasi M (2019) Environment Land use change, urbanization, and change in landscape pattern in a metropolitan area. Sci Total Environ 655:707–719. https://doi.org/10.1016/j.scitotenv.2018.11.267

Darabi H, Choubin B, Rahmati O, Haghighi AT et al (2019) Urban flood risk mapping using the GARP and QUEST models: a comparative study of machine learning techniques. J of hydr 569:142–154

Darabi H, Haghighi AT, Mohamadi MA et al (2020) Urban flood risk mapping using data-driven geospatial techniques for a flood-prone case area in Iran. Hydrol Res 51:127–142

Duncan JMA, Boruff B, Saunders A et al (2019) Turning down the heat : an enhanced understanding of the relationship between urban vegetation and surface temperature at the city scale. Sci Total Environ 656:118–128. https://doi.org/10.1016/j.scitotenv.2018.11.223

FAO (2015) Impact of natural hazards and disasters on agriculture and food security and nutrition. FAO Rep 16

Fotheringham AS, Charlton ME, Brunsdon C (1998) Geographically weighted regression: a natural evolution of the expansion method for spatial data analysis. Environ Plan A 30:1905–1927

Gaston KJ, Warren PH, Thompson K, Smith RM (2005) Urban domestic gardens (IV): the extent of the resource and its associated features. Biodivers Conserv 14:3327–3349

Georganos S, Abdi AM, Tenenbaum DE, Kalogirou S (2017) Examining the NDVI-rainfall relationship in the semi-arid Sahel using geographically weighted regression. J Arid Environ 146:64–74. https://doi.org/10.1016/j.jaridenv.2017.06.004

Giang PQ, Trang NTM, Anh TTH, Binh NT (2020) Prediction of economic loss of rice production due to flood inundation under climate change impacts using a modeling approach: a case study in Ha Tinh Province. Vietnam Clim Change 6:52–63

Haghighi AT, Darabi H, Shahedi K et al (2020) A scenario-based approach for assessing the hydrological impacts of land use and climate change in the Marboreh watershed. Iran Environ Model Assess 25:41–57

Hoekstra AY (2003) Virtual water: an introduction. In: Virtual water trade. Proceedings of the international expert meeting on virtual water trade. Value of water research report series, vol 11, pp 13–23

Hoekstra AY (2009) Human appropriation of natural capital: a comparison of ecological footprint and water footprint analysis. Ecol Econ 68:1963–1974

Hoekstra AY (2017) Water footprint assessment: evolvement of a new research field. Water Resour Manag 31:3061–3081

Hosseini FS, Choubin B, Mosavi A et al (2020) Flash-flood hazard assessment using ensembles and Bayesian-based machine learning models: application of the simulated annealing feature selection method. Sci Total Environ 711:135161

Kalota D (2017) Exploring relation of land surface temperature with selected variables using geographically weighted regression and ordinary least square methods in Manipur State, India. Geocarto Int 32:1105–1119. https://doi.org/10.1080/10106049.2016.1195883

Karizaki VM (2016) Ethnic and traditional Iranian rice-based foods. J Ethn Foods 3:124–134

Kavian A, Mohammadi M, Gholami L, Rodrigo-Comino J (2018) Assessment of the spatiotemporal effects of land use changes on runoff and nitrate loads in the Talar river. Water 10:445

Kazakis N, Kougias I, Patsialis T (2015) Assessment of flood hazard areas at a regional scale using an index-based approach and analytical hierarchy process: application in Rhodope-Evros region, Greece. Sci Total Environ 538:555–563

Khaleghi MR (2017) The influence of deforestation and anthropogenic activities on runoff generation. J For Sci 63:245–253

Khosravi K, Nohani E, Maroufinia E, Pourghasemi HR (2016) A GIS-based flood susceptibility assessment and its mapping in Iran: a comparison between frequency ratio and weights-of-evidence bivariate statistical models with multi-criteria decision-making technique. Nat Hazards 83:947–987

Kourgialas NN, Karatzas GP (2011) Flood management and a GIS modelling method to assess flood-hazard areas—a case study. Hydrol Sci J 56:212–225

Kourgialas NN, Karatzas GP (2016) A flood risk decision making approach for Mediterranean tree crops using GIS; climate change effects and flood-tolerant species. Environ Sci Policy 63:132–142

Li H, Liu Y, Zhang A (2018) Spatially varying associations between creative worker concentrations and social diversity in Shenzhen, China. Qual Quant 52:85–99. https://doi.org/10.1007/s11135-016-0451-x

Lloyd CD (2005) Assessing the effect of integrating elevation data into the estimation of monthly precipitation in Great Britain. J Hydrol 308:128–150

Maghsood FF, Moradi H, Bavani M et al (2019) Climate change impact on flood frequency and source area in northern Iran under CMIP5 scenarios. Water 11:273

Mekonnen MM, Hoekstra AY (2011) The green, blue and grey water footprint of crops and derived crop products. Hydrol Earth Syst Sci Discuss 8:763–809

Mind'je R, Li L, Amanambu AC et al (2019) Flood susceptibility modeling and hazard perception in Rwanda. Int J Disaster Risk Reduct 38:101211

Morgan RPC (2005) Soil erosion and conservation, 3rd edn. Blackwell Publ, Oxford

Nejad MR, Rostami K, Emami MH et al (2011) Epidemiology of celiac disease in Iran: a review. Middle East J Dig Dis 3:5

Ozkan SP, Tarhan C (2016) Detection of flood hazard in urban areas using GIS: izmir case. Procedia Technol 22:373–381

Pacetti T, Caporali E, Rulli MC (2017) Floods and food security: a method to estimate the effect of inundation on crops availability. Adv Water Resour 110:494–504

Pirnia A, Darabi H, Choubin B et al (2019) Contribution of climatic variability and human activities to stream flow changes in the Haraz River basin, northern Iran. J Hydro-environment Res 25:12–24

Purwaningsih T, Prajaningrum CS, Anugrahwati M (2018) Building model of flood cases in central java province using geographically weighted regression (GWR). Int J Appl Bus Inf Syst 2:14–27

Rahmati O, Zeinivand H, Besharat M (2016) Flood hazard zoning in Yasooj region, Iran, using GIS and multi-criteria decision analysis. Geomat Nat Hazards Risk 7:1000–1017

Rahmati O, Darabi H, Haghighi AT et al (2019) Urban flood hazard modeling using self-organizing map neural network. Water 11:2370

Sadeghi-Pouya A, Nouri J, Mansouri N, Kia-Lashaki A (2017) An indexing approach to assess flood vulnerability in the western coastal cities of Mazandaran. Iran. Int J disaster risk Reduct 22:304–316

Salimi S, Balyani S, Asaad S et al (2018) The prediction of spatial and temporal distribution of precipitation regime in Iran : the case of Fars province. Model Earth Syst Environ 4:565–577. https://doi.org/10.1007/s40808-018-0451-z

Santos PP, Reis E, Pereira S, Santos M (2019) A flood susceptibility model at the national scale based on multicriteria analysis. Sci Total Environ 667:325–337

Shooshtari SJ, Gholamalifard M (2015) Scenario-based land cover change modeling and its implications for landscape pattern analysis in the Neka Watershed. Iran Remote Sens Appl Soc Environ 1:1–19

Sim J-S, Kim J-S, Lee S-H (2014) Local Analysis of the spatial characteristics of urban flooding areas using GWR. J Environ Impact Assess 23:39–50

Smith C, Dawson D, Archer J et al (2011) From green to grey; observed changes in garden vegetation structure in London, 1998–2008. London Wildl Trust, London

Stewart Fotheringham A, Charlton M, Brunsdon C (1996) The geography of parameter space: an investigation of spatial non-stationarity. Int J Geogr Inf Syst 10:605–627

Taghipour Javi S, Malekmohammadi B, Mokhtari H (2014) Application of geographically weighted regression model to analysis of spatiotemporal varying relationships between groundwater quantity and land use changes (case study: Khanmirza Plain, Iran). Environ Monit Assess 186:3123–3138. https://doi.org/10.1007/s10661-013-3605-5

Tehrany MS, Pradhan B, Mansor S, Ahmad N (2015) Flood susceptibility assessment using GIS-based support vector machine model with different kernel types. CATENA 125:91–101

Torabi Haghighi A, Menberu MW, Darabi H et al (2018) Use of remote sensing to analyse peatland changes after drainage for peat extraction. L Degrad Dev 29:3479–3488

Tu J (2011) Spatially varying relationships between land use and water quality across an urbanization gradient explored by geographically weighted regression. Appl Geogr 31:376–392. https://doi.org/10.1016/j.apgeog.2010.08.001

Wang C, Du S, Wen J et al (2017) Analyzing explanatory factors of urban pluvial floods in Shanghai using geographically weighted regression. Stoch Environ Res Risk Assess 31:1777–1790

Warhurst JR, Parks KE, McCulloch L, Hudson MD (2014) Front gardens to car parks: changes in garden permeability and effects on flood regulation. Sci Total Environ 485:329–339

Wu SS, Yang H, Guo F, Han RM (2017) Spatial patterns and origins of heavy metals in Sheyang River catchment in Jiangsu, China based on geographically weighted regression. Sci Total Environ 580:1518–1529. https://doi.org/10.1016/j.scitotenv.2016.12.137

Xia F, Qu L, Wang T et al (2018) Distribution and source analysis of heavy metal pollutants in sediments of a rapid developing urban river system. Chemosphere 207:218–228. https://doi.org/10.1016/j.chemosphere.2018.05.090

Zerger A (2002) Examining GIS decision utility for natural hazard risk modelling. Environ Model Softw 17:287–294

Zhao C, Jensen J, Weng Q, Weaver R (2018) A geographically weighted regression analysis of the underlying factors related to the surface urban heat island phenomenon. Remote Sens 10:1–18. https://doi.org/10.3390/rs10091428

Affiliations

Maziar Mohammadi[1] · Hamid Darabi[2] · Fahimeh Mirchooli[1] · Alireza Bakhshaee[3] · Ali Torabi Haghighi[2]

Maziar Mohammadi
maziarmohammadi68@yahoo.com

Fahimeh Mirchooli
fahimeh.mirchooli@gmail.com

Alireza Bakhshaee
alireza.bakhshaee@studio.unibo.it

[1]   Department of Watershed Management Engineering, Faculty of Natural Resources and Marine Sciences, Tarbiat Modares University, Noor, Iran

2   Water, Energy and Environmental Engineering Research Unit, University of Oulu, P.O. Box 4300, FIN-90014 Oulu, Finland

3   Department of Civil, Chemical, Environmental and Material Engineering, University of Bologna, Bologna, Italy